Journal of Materials Chemistry

Dynamic Article Links

Cite this: *J. Mater. Chem.*, 2012, **22**, 20394

www.rsc.org/materials

PAPER

Novel triphenylamine-containing ambipolar polyimides with pendant anthraquinone moiety for polymeric memory device, electrochromic and gas separation applications†

Yi-Cheng Hu,[a] Chih-Jung Chen,[a] Hung-Ju Yen,[a] Kun-Ying Lin,[a] Jui-Ming Yeh,[b] Wen-Chang Chen[ac] and Guey-Sheng Liou*[a]

Received 22nd May 2012, Accepted 10th August 2012
DOI: 10.1039/c2jm33266c

Novel electron-donating triphenylamine (TPA)-containing electroactive functional polyimides with electron-withdrawing pendant anthraquinone moiety were designed and prepared for memory devices, electrochromic and gas separation applications. These high-performance polymers exhibited two conductivity states and could be swept negatively with a high ON/OFF current ratio of 10^9. The ON state of **OAQ-6FPI** polyimide remained around 8 min after removing the applied voltage, while the **AQ-6FPI** polyimide quickly returned to the OFF state during the backward sweep in a dual sweep process, implying that devices based on **OAQ-6FPI** and **AQ-6FPI** reveal static random access memory (SRAM) and dynamic random access memory (DRAM) behaviors resulting from the isolated donor–acceptor (D–A) and non-isolated D–A structures, respectively. Meanwhile, the polymer films exhibited electrochromic characteristics with a color change from neutral colorless or pale yellowish to blue and green at applied potentials, ranging from 0.00 to 1.40 V. Furthermore, the presence of a bulky and carbonyl-containing anthraquinone unit could enhance effectively CO_2 permeability coefficients (PCO_2) and permeability selectivity (PCO_2/PCH_4) for these polyimide membranes in the range of 21.6–69.9 and 28.8–31.7, respectively, and permeability increased with higher efficiency by directly attaching the bulky group to the backbone than incorporating *via* a spacer.

Introduction

Nowadays, the utilization of polymeric material in electronic devices has attracted extensive attention, such as light-emitting diodes,[1] transistors,[2] and solar cells.[3] Donor–acceptor (D–A) containing polymers include both electron donor and acceptor moieties within a repeating unit, which can be switched between two conductive states *via* an electrical field and have been widely researched recently for resistive switching memory applications.[4] Based on the advantages of convenient and low-cost device fabrication by using a solution process, three-dimensional stacking capability and well structural flexibility,[5] electrically bistable resistive switching device based on polymeric materials have significant advantages over inorganic silicon- and metal-oxide-based memory materials.[5b] Among the researched polymeric systems, charge transfer (CT) effect is one of the interesting mechanisms to induce the RRAM (resistor-type polymer memory) behavior by introducing the electron donor and the electron acceptor moiety into the repeat unit of the polymer. Under an applied electric field, the charge transfer will occur which means transfer of the electronic charge from the donor to the acceptor moiety, and the resulting structure can be defined as CT complex (CTC).[6] The stability of the CTC is regarded as one of the crucial factors for its memory behavior. The importance of structural effects tuned by incorporating different substituents into electron donating moieties on the relaxation time of the polymeric memory was investigated by Kang's and Ree's work; the devices fabricated by TPA-based polyimide **TPA-6FPI**[4a] exhibited volatile DRAM behavior, while both phenylamine-substituted and hydroxy-substituted TPA-containing polyimide (**6F-2TPA PI**)[7a] and (**6F-HTPA PI**)[7b] demonstrated a non-volatile write-once-read-many-times (WORM) property. Besides, the characteristic of polymer memory can move from DRAM to SRAM and even become WORM or flash type non-volatile memory behavior by increasing the dipole moment of the polymers.[4j,8] Moreover, the linkage group effects between donor and acceptor moieties also play a key factor in influencing the time interval from CT state to the original state due to the conformational changes between the

[a]*Institute of Polymer Science and Engineering, National Taiwan University, 1 Roosevelt Road, 4th Sec., Taipei 10617, Taiwan. E-mail: gsliou@ntu.edu.tw*
[b]*Department of Chemistry and Center for Nanotechnology and R&D Center for Membrane Technology, Chung-Yuan Christian University, Chung Li 32023, Taiwan*
[c]*Department of Chemical Engineering, National Taiwan University, 1 Roosevelt Road, 4th Sec., Taipei 10617, Taiwan*
† Electronic supplementary information (ESI) available. See DOI: 10.1039/c2jm33266c

donor and acceptor moiety induced by charge transfer, that could increase the torsional displacement and produce a potential energy barrier for the back charge transfer to the ground state, thus extending the retention time of the ON state.[4j,8c,9] For example, both **OXTA-PI**[9a] and **AZTA-PI**[9b] containing pendent TPA donor exhibited WORM memory characteristic in Al/polymer/ITO sandwich devices due to the orthogonal overlap in orbitals between acceptor and pendent donor which could create a higher energy barrier for back charge transfer, therefore maintaining the device in the ON state after removing the applied electrical field.

Aromatic polymers containing a TPA moiety such as polyimide (PI) and polyamide (PA)[4j] are favorable functional materials not only for memory devices due to their intrinsic excellent thermal dimensional and high ON/OFF ratio, but also electrochromic application[10] resulting from the electron-rich triarylamines which can be easily oxidized to form stable radical cations, and the oxidation process is always associated with a noticeable change of coloration. Recently, multi-functional high performance polyimides have been designed for various applications in each polymeric material, such as methyl-substituted TPA-containing polyimides prepared for polymer memory, and electrochromic and gas separation application have been reported.[11] Furthermore, triphenylethylene containing polyimide with fluorescent and resistive switching characteristics has been designed and synthesized.[12] The philosophy for designing multifunctional material can also be extended to other novel high performance polymer systems.

In this study, in order to obtain solution-processable polyimides for polymeric memory, electrochromic and gas separation applications, we synthesized two series of polyimides **AQ-PIs** and **OAQ-PIs** from diamines 2-(bis(4-aminophenyl)amino) anthracene-9,10-dione (**1**), and 2-(4-(bis(4-aminophenyl)amino) phenoxy)anthracene-9,10-dione (**2**), respectively. The general properties such as solubility, crystallinity, and thermal properties are described. The TPA-containing polyimides **AQ-6FPI** and **OAQ-6FPI** were used to fabricate the memory devices. In addition to the phthalimide acceptor moiety in the main chain, the pendant anthraquinone as a stronger acceptor group was also introduced to TPA *via* an ether linkage or directly attached into the backbone, which is different from the previous research discussing the memory behavior only having a single donor–acceptor effect from the main chain of the polyimide system. The effect of dual acceptor moieties both in the main chain and side chain on memory behavior was investigated in this work, and the electron withdrawing capability of these two acceptors could be verified by electrochemical and spectroelectrochemical behavior. The memory devices were prepared with configurating the ITO/polymer/Al, and the memory properties were investigated by *I–V* measurements. The electrochemical, electrochromic, and gas separation properties of these polymers are also described herein and are compared with each other.

Experimental

Materials

2-(Bis(4-aminophenyl)amino)anthracene-9,10-dione (**1**) and 2-(4-(bis(4-aminophenyl)amino)phenoxy)anthracene-9,10-dione (**2**) were synthesized according to the literature.[13] Acetonitrile (CH_3CN), *N*,*N*-dimethylformamide (DMF) (ACROS), dimethyl sulfoxide (DMSO), *N*,*N*-dimethylacetamide (DMAc) (TEDIA), and tetrahydrofuran (THF) were used without further purification. 2,2-Bis(3,4-dicarboxyphenyl)hexafluoropropane dianhydride (6FDA) (Chriskev), 3,3′,4,4′-diphenylsulfonetetracarboxylic dianhydride (DSDA) (TCI) was purified by vacuum sublimation. Tetrabutylammonium perchlorate (TBAP) (ACROS) was recrystallized twice using ethyl acetate under nitrogen atmosphere and then dried *in vacuo* prior to use. All other reagents were used as received from commercial sources.

Polymer synthesis

Aromatic polyimides **AQ-PIs** and **OAQ-PIs** could be prepared by the one-step polycondensation of diamines **1** and **2** with 2-bis(3,4-dicarboxyphenyl)hexafluoropropane dianhydride and 3,3′,4,4′-diphenylsulfonetetracarboxylic dianhydride, respectively, in *m*-cresol in the presence of isoquinoline (Scheme 1), all polymerization reactions proceeded homogenously and with high viscosity. The synthesis of polyimide **AQ-6FPI** was used as an example to illustrate the general synthetic route used to produce the polyimides. The homogeneous mixture of diamine **1** (0.4055 g, 1.00 mmol), dianhydride 6FDA (0.4442 g, 1.00 mmol), and 0.32 mL isoquinoline in *m*-cresol (3 mL) was stirred at room temperature under nitrogen atmosphere for 10 h, and then heated to 185 °C for 18 h. The resulting mixture was allowed to cool to room temperature, and the viscous solution was poured slowly into 200 mL of methanol with stirring. The precipitated polymer was collected using filtration, washed thoroughly with hot methanol and dried under vacuum at 100 °C for 15 h. The inherent viscosity of the obtained polyimide **AQ-6FPI** was 0.49 dL g^{-1} (measured at a concentration of 0.5 g dL^{-1} in DMAc at 30 °C). The formation of the polyimide was confirmed by IR spectroscopy (as shown in Fig. S1 in the ESI†). The IR spectra of **AQ-6FPI** exhibited characteristic imide absorption bands at around 1781 (asymmetrical C═O), 1720 (symmetrical C═O), 1380 (C–N), and 738 cm^{-1} (imide ring deformation) anal. calcd for $(C_{47}H_{27}F_6N_3O_6)_n$ $(843.72)_n$: C, 66.91%; H, 3.23%; N, 4.98%. Found: C, 68.47%; H, 3.35%; N, 5.26%.

Measurements

Elemental analysis was run in a Heraeus VarioEL-III CHNS elemental analyzer. The inherent viscosities were determined at 0.5 g dL^{-1} concentration using Tamson TV-2000 viscometer at 30 °C. Thermogravimetric analysis (TGA) was conducted with a PerkinElmer Pyris 1 TGA. Experiments were carried out on approximately 6–8 mg film samples heated in flowing nitrogen or air (flow rate = 20 cm^3 min^{-1}) at a heating rate of 20 °C min^{-1}. DSC analyses were performed on a PerkinElmer Pyris 1 DSC at a scan rate of 10 °C min^{-1} in flowing nitrogen (20 cm^3 min^{-1}). The gas permeability of the polymer membranes with thickness around 50–90 μm was measured with a model GTR-10 gas permeability analyzer (Yanagimoto, Kyoto, Japan), which consists of upstream and downstream parts separated by a membrane. The gases measured include O_2, N_2, CO_2, and CH_4. The pressure on one face of the free-standing film (or called membrane) was kept at 294 kPa, and the other face was at zero

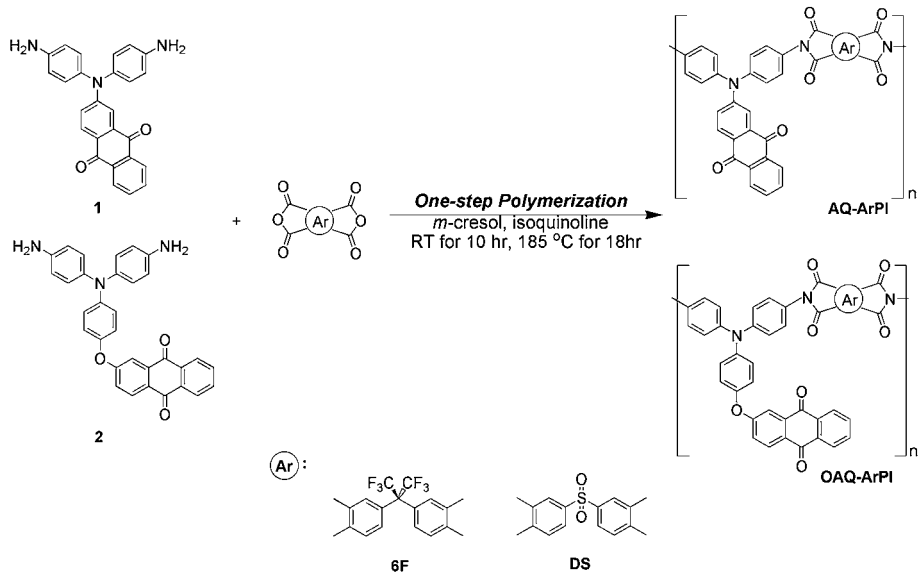

Scheme 1 Polymer synthesis of **AQ-PIs** and **OAQ-PIs**.

pressure initially to allow the gas to permeate through the free-standing film. The rate of gas transmission was obtained using gas chromatography, from which gas permeability was calculated.

Measurements of cyclic voltammetry and spectroelectrochemistry

Cyclic voltammetry (CV) was performed with a Bioanalytical System Model CV-27 and conducted with the use of a three-electrode cell in which ITO (polymer films area about 0.5 cm × 1.2 cm) was used as a working electrode and a platinum wire as an auxiliary electrode at a scan rate of 50 mV s^{-1} against a Ag/AgCl reference electrode in anhydrous DMF and CH_3CN, using 0.1 M of TBAP as a supporting electrolyte in nitrogen atmosphere. All cell potentials were taken using a homemade Ag/AgCl, KCl (sat.) reference electrode. Spectroelectrochemical experiments were carried out in a cell built from a 1 cm commercial UV-visible cuvette using Hewlett-Packard 8453 UV-visible diode array spectrophotometer. The ITO-coated glass slide was used as the working electrode, a platinum wire as the counter electrode, and Ag/AgCl cell as the reference electrode.

Fabrication and measurement of the memory device

The memory device was fabricated with the configuration of ITO/polymer/Al as shown in Fig. 1. The ITO glass used for the memory device was cleaned by ultrasonication with water, acetone, and isopropanol each for 15 min. A 250 μL DMAc solution of **AQ-6FPI** or **OAQ-6FPI** (23–25 mg mL^{-1}) was first filtered through 0.45 μm pore size of PTFE membrane syringe filter, then the filtered solution was spin-coated onto the ITO glass at a rotation rate of 1000 rpm for 60 s and heated at 100 °C for 10 min under nitrogen. The film thickness was determined to be around 50 nm. Finally, a 300 nm-thick Al top electrode was thermally evaporated through the shadow mask (recorded device units of 0.5 × 0.5 mm^2 in size) at a pressure of 10^{-7} Torr with a depositing rate of 3–5 Å s^{-1}. The electrical characterization of the memory device was performed by a Keithley 4200-SCS semiconductor parameter analyzer equipped with a Keithely 4205-PG2 arbitrary waveform pulse generator. ITO was used as the cathode (maintained as common), and Al was set as the anode during the voltage sweep. The probe tip of a tinned copper shaft with a point radius <0.1 μm was attached to 10 μm diameter tungsten wire (GGB Industries, Inc.).

Molecular simulation

The Gaussian 09 program package is used for theoretical calculation in this research, and the basic units of **AQ-6FPI** and **OAQ-6FPI** were optimized by means of the density functional theory (DFT) method at the B3LYP level of theory (Beckesstyle three-parameter density functional theory using the Lee–Yang–Parr correlation functional) with the 6-31 G(d) basic set.

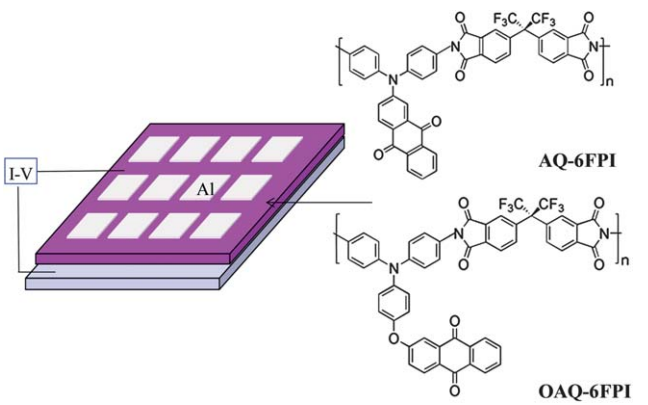

Fig. 1 Molecular structure of **AQ-6FPI** and **OAQ-6FPI** and a schematic diagram of the memory device consisting of a polymer thin film sandwiched between an ITO bottom electrode and an Al top electrode. The thickness of the polymer film is about 50 nm and the thickness of the electrode is 300 nm.

Results and discussion

Polymer synthesis

Polymers **AQ-6FPI**, **AQ-DSPI**, **OAQ-6FPI**, and **OAQ-DSPI** were synthesized from diamine **1** and **2** *via* one-step high temperature polycondensation, and all obtained polyimides with high enough molecular weight to afford flexible films. The inherent viscosities, weight-average molecular weights (M_w), and polydispersity (PDI) of these resulting polyimides are summarized in Table 1.

Basic characterization and thermal properties

The solubility behavior of these polymers was investigated qualitatively, and the results are listed in Table 2. These polyimides exhibited higher solubility in polar aprotic organic solvents such as NMP and DMAc due to the introduction of the bulky pendant groups. Polyimides **AQ-6FPI** and **OAQ-6FPI** could even be dissolved in less polar solvents such as THF and $CHCl_3$; their excellent solubility can be attributed to the existence of the additional bulky hexafluoroisopropylidene units which reduce the intermolecular interaction and suppress the CTC formation. The thermal properties of these polyimides are summarized in Table 3. Typical TGA curves of **AQ-PIs** and **OAQ-PIs** are depicted in Fig. S2.† All of the polyimides showed outstanding thermal stability; the 10% weight-loss temperatures of the polyimides in nitrogen and air were recorded in the range of 520–630 °C and 540–610 °C, respectively. The amount of carbonized residue (char yield) of these polymers in nitrogen atmosphere was more than 60% at 800 °C; the high char yields of these polymers can be ascribed to their high aromatic content. The glass-transition temperatures (T_g) measured by the DSC thermograms were observed in the range of 275–300 °C depending upon the stiffness and rigidity of the polyimide chain.

Electrochemical properties

The electrochemical behavior of the polyimides **AQ-PIs** and **OAQ-PIs** was investigated using cyclic voltammetry (CV) conducted for the cast film on an indium-tin oxide (ITO)-coated glass slide as working electrode in anhydrous acetonitrile and DMF, using 0.1 M of TBAP as a supporting electrolyte under nitrogen atmosphere, and the results are summarized in Table 4. The typical reduction cyclic voltammograms of polyimides **AQ-6FPI** and **OAQ-6FPI** are depicted in Fig. 2(a) and (b), respectively, meanwhile the results of the corresponding **DSPIs** are shown in Fig. S3† for comparison. The first half-wave potentials ($E_{1/2}$) of the reduction process were −0.79 and −0.8 V for **OAQ-6FPI** and **AQ-6FPI**, respectively, which could be attributed to the reduction of anthraquinone unit;[13] and the second half-wave potentials ($E_{1/2}$) of the reduction process were −1.17 and −1.28 V derived from the phthalimide moieties, respectively. Furthermore, the third reduction half-wave potential ($E_{1/2}$) was −1.49 V for **OAQ-6FPI**, attributing to the second reduction of anthraquinone unit.

Table 1 Inherent viscosity and molecular weights of polyamides

Code	η_{inh}[a] (dL g^{-1})	M_w[b]	M_n[b]	PDI[c]
AQ-DSPI	0.56	159 000	70 000	2.3
AQ-6FPI	0.49	169 000	70 500	2.4
OAQ-DSPI	0.57	169 000	81 000	2.1
OAQ-6FPI	0.59	180 000	75 000	2.4

[a] Measured at a polymer concentration of 0.5 g dL^{-1} in DMAc at 30 °C. [b] Calibrated with polystyrene standards, using NMP as the eluent at a constant flow rate of 1 mL min^{-1} at 40 °C. [c] Polydispersity index (M_w/M_n).

Table 2 Solubility behavior of polyimides

	Solvent[a]						
Code	NMP	DMAc	DMF	DMSO	*m*-Cresol	THF	$CHCl_3$
AQ-DSPI	++	++	±	–	++	–	–
AQ-6FPI	++	++	+	–	++	++	++
OAQ-DSPI	++	++	±	–	++	–	–
OAQ-6FPI	++	++	+	–	++	++	++

[a] Qualitative solubility was tested with 5 mg of a sample in 1 mL of stirred solvent. ++, soluble at room temperature; +, soluble on heating; ±, partially soluble; –, insoluble even on heating.

Memory device characteristics of the OAQ-6FPI and AQ-6FPI

Fig. 3(a) exhibits the current–voltage result of **AQ-6FPI**; the device was switched to ON state at a threshold voltage about −3.5 V (line 1) and subsequently reset to OFF state just after removing the applied electrical field without any erasing process, and the device could be turned on again at about −3.4 V during the second negative sweep (line 2), indicating DRAM property for this **AQ-6FPI** memory device. Besides, the device remained at low-conductivity (OFF) state when it was conducted by positive bias. Furthermore, the behavior of dual sweep current–voltage of **AQ-6FPI** is depicted in Fig. 4(a); the device could be set to ON state at a threshold voltage of about −3.5 V and reset to OFF state at around −1.9 V during the backward sweep of the dual sweep process, implying the instability of the CT state of **AQ-6FPI**. Fig. 3(b) depicts the current–voltage result of **OAQ-6FPI**, the current increasing from 10^{-13} to 10^{-14} to 10^{-4} to 10^{-5} (high-conductivity state) instantaneously at the threshold

Table 3 Thermal properties of polyimides

		T_d at 5% weight loss[b] (°C)		T_d at 10% weight loss[b] (°C)		
Polymer	T_g[a] (°C)	N_2	Air	N_2	Air	Char yield[c] (wt%)
AQ-DSPI	305	490	495	530	560	62
AQ-6FPI	330	600	585	630	610	60
OAQ-DSPI	275	520	515	560	570	62
OAQ-6FPI	275	580	540	620	590	65

[a] Midpoint temperature of the baseline shift on the second DSC heating trace (rate = 20 °C min^{-1}) of the sample after quenching from 400 to 50 °C (rate = 200 °C min^{-1}) in nitrogen. [b] Decomposition temperature, recorded *via* TGA at a heating rate of 20 °C min^{-1}. [c] Residual weight percentage at 800 °C in nitrogen.

Table 4 Redox potentials and energy levels of polyimides[a]

Code	Thin films (nm)		Oxidation[b]	Reduction[c]			Energy level		
	λ_{max}	λ_{onset}	$E_{1/2}$ (V)	$E_{1/2}$ (V)	E_g^{EC} (eV)	E_g^{Opt} (eV)	$HOMO^{EC}$[d] (eV)	$LUMO^{Opt}$ (eV)	$LUMO^{EC}$ (eV)
AQ-DSPI	308	566	1.29	−0.79	2.08	2.19	5.65	3.46	3.57
AQ-6FPI	314	563	1.31	−0.80	2.11	2.20	5.67	3.48	3.56
OAQ-DSPI	309	582	1.09	−0.78	1.87	2.13	5.45	3.32	3.58
OAQ-6FPI	317	566	1.11	−0.78	1.89	2.19	5.47	3.28	3.58

[a] E_g^{EC} (electrochemical band gap): difference between $HOMO^{EC}$ and $LUMO^{EC}$. E_g^{Opt} (optical band gap): calculated from polymer films ($E_g = 1240/\lambda_{onset}$). $LUMO^{Opt}$ (LUMO energy levels calculated from optical method): difference between $HOMO^{EC}$ and E_g^{Opt}. [b] *vs.* Ag/AgCl in CH_3CN. [c] *vs.* Ag/AgCl in DMF. [d] The HOMO and LUMO energy levels were calculated from cyclic voltammetry and were referenced to ferrocene (4.8 eV).

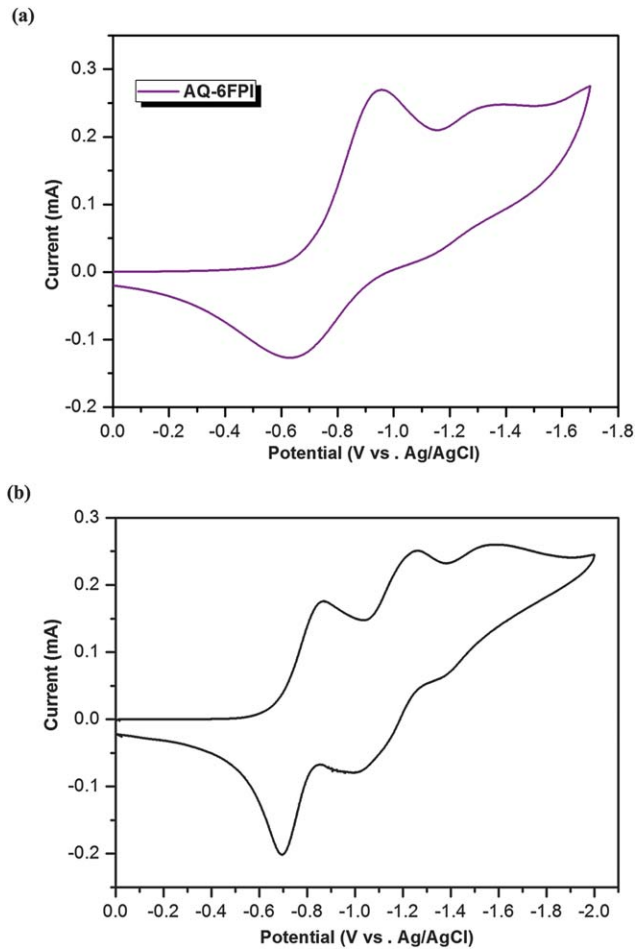

Fig. 2 Cyclic voltammetric diagrams of polyimide (a) **AQ-6FPI** and (b) **OAQ-6FPI** films on an ITO-coated glass substrate over cyclic scans in 0.1 M TBAP/DMF at a scan rate of 50 mV s^{-1}.

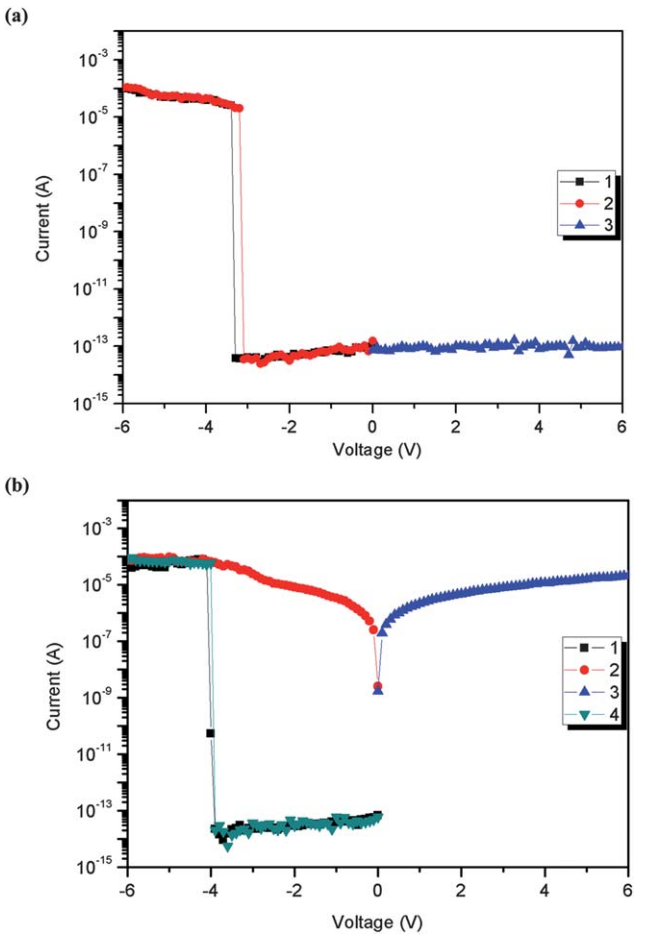

Fig. 3 (a) Current–voltage (*I–V*) characteristics of the ITO/**AQ-6FPI**/Al memory device (the time interval between the first and second sweep is less than 5 s), (b) current–voltage (*I–V*) characteristics of the ITO/**OAQ-6FPI**/Al memory device (the time interval between the third and fourth sweep is 8 min).

voltage of −3.9 V in the first negative sweep (line 1), indicating the writing process for the transition from the OFF state to the ON state. The device remained in the ON state during the subsequent negative scan (line 2) and the subsequent positive scan (line 3) which could be defined as the reading process. After turning off the power for 8 min, the memory device returned to OFF state without any erasing process, and could be switched on again at threshold voltage −3.9 V (line 4); this phenomenon revealed that the memory device possessed SRAM property. Moreover, the effect of the operation time on the ON and OFF states of the ITO/**OAQ-6FPI**/Al device with continuous −2 V was investigated as shown in Fig. 4(b), and no obvious degradation in current could be observed at both ON and OFF states for at least 10^4 s in the readout test, revealing the excellent stability of this device.

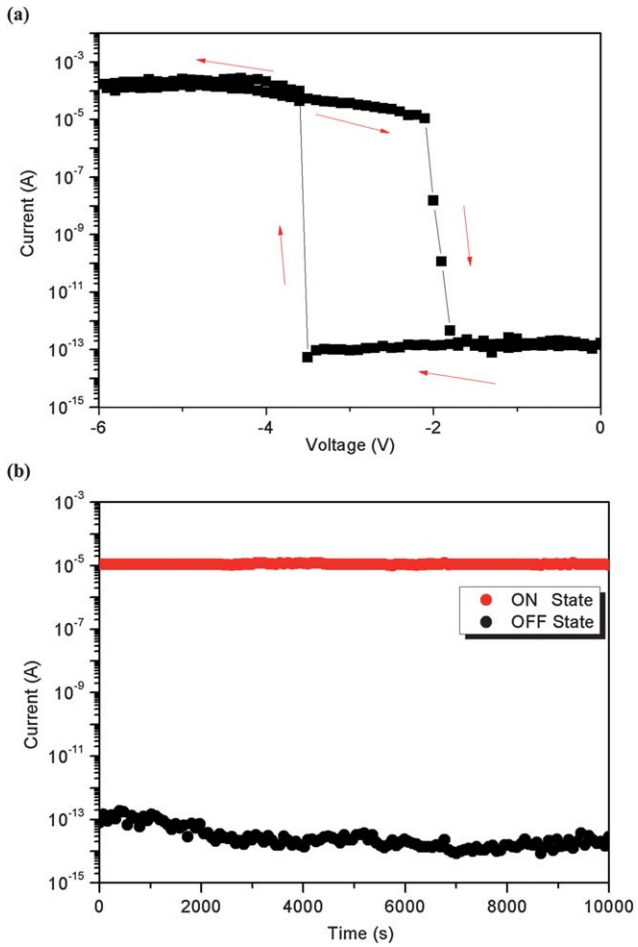

Fig. 4 (a) Dual sweep current–voltage (*I–V*) characteristics of the ITO/**AQ-6FPI**/Al memory device. (Each dual sweep process will turn to off state during the backward sweep.) (b) Effect of operation time on the ON and OFF states of the ITO/**OAQ-6FPI**/Al device with a continuing −2 V.

Switching mechanism of the OAQ-6FPI and AQ-6FPI

For getting more understanding of the memory behavior of the present **OAQ-6FPI** and **AQ-6FPI** devices, the molecular orbital and electrostatic potential surface (ESP) of the basic units were estimated by performing molecular simulation, and the results are illustrated in Fig. 5. These two systems with a similar molecular orbital location (charge density distribution) shown in Fig. 5 indicated that these two systems could proceed via a similar charge transfer route from TPA donor to the pendant anthraquinone acceptor. During the negative voltage sweep, both **AQ-6FPI** and **OAQ-6FPI**, with analogous charge density distribution, proceed via a similar charge transfer pathway from TPA donor to the pendent AQ acceptor as the applied potential reaches the switching-on voltage. Some electrons at the HOMO may accumulate energy then overcome the band gap, thus transiting to the LUMO+4 resulting in an excited state. On the other hand, electrons at the HOMO could also be excited to other LUMOs with a lower energy barrier. Therefore, charge transfer could occur through several routes such as indirectly from the LUMO+3 or LUMO+2 through intermediate LUMO+1 and then to the LUMO, or from the intermediate LUMO+1 to the LUMO, and even directly from the HOMO to the LUMO to form conductive charge transfer complexes. In addition, during the intra- or intermolecular charge transfer induced by the applied electric field, the generating holes can be delocalized within TPA moieties resulting in a conducting channel in the polymer chain, then facilitate the migration of charge carriers (holes). However, the different memory properties of these two systems could be contributed to the isolated effect and the non-coplanar geometry of CT complex between the TPA donor and the acceptor moieties for the **OAQ-6FPI** when compared with **AQ-6FPI**; the ether linkage between donor and pendant anthraquinone acceptor in **OAQ-6FPI** can efficiently inhibit the intramolecular backward route, thus stabilizing the CT complex and resulting in a much longer retention time than the **AQ-6FPI** system.

Spectroelectrochemistry

Because the energy levels of LUMO+1 (phthalimide moiety) and LUMO (anthraquinone moiety) were too close to be distinguished from the results of simulation, the spectroelectrochemical measurements were used to evaluate and compare the electron-withdrawing capability between these two moieties for demonstrating the above switching mechanism. The spectroelectrochemical behavior of polyimide **OAQ-6FPI** film is presented in Fig. 6(a) as UV-vis-NIR absorbance curves correlated to applied potentials. By applying the reduction potential of −0.8 V (the first stage reduction potential of polyimide **OAQ-6FPI**), an increasing intensity of the absorption peaks at 555 and 894 nm could be observed. For comparison, the corresponding polyimide **TPA-6FPI**[10a] shown in Fig. 6(b) was used to get more conclusive evidence about the reductive capability between the anthraquinone and phthalimide moieties; at the reduction potential of −0.8 V, no obvious UV-vis-NIR absorbance change could be observed, and an apparent absorption change in the UV-vis region from 300 to 450 nm could be found only until the reduction potential was increased to −1.3 V, implying the reduction of the imide ring requires a higher electrical potential. Thus, we confirmed the first stable anion radical from UV-vis-NIR spectral changes should be derived from the anthraquinone moiety for **OAQ-6FPI**.[13]

Electrochromic characterization

The electrochromic behavior of polyimide **AQ-DSPI** and **OAQ-DSPI** films is presented in Fig. 7(a) and (b) as a series of UV-vis-NIR absorbance curves correlated to applied potentials. In the neutral form (0 V), the film exhibited strong absorption at 308 nm for **AQ-DSPI** and 309 nm for **OAQ-DSPI**, representing the characteristic absorption of a neutral triarylamine unit. In addition, **AQ-DSPI** had a shoulder peak at 468 nm due to the strong D–A charge transfer interaction system. Upon oxidation, new peaks at 365 and 765 nm gradually increased in intensity for polymer **AQ-DSPI**, and two new absorption peaks at 372 and 750 nm grew up for polymer **OAQ-DSPI** due to the formation of a stable radical cation of the TPA moieties. The film color changes are also displayed in the inset of Fig. 7(a) and (b); **AQ-DSPI** with a strong D–A system exhibits a pale brownish neutral state to the green color oxidized form, while **OAQ-DSPI** with an

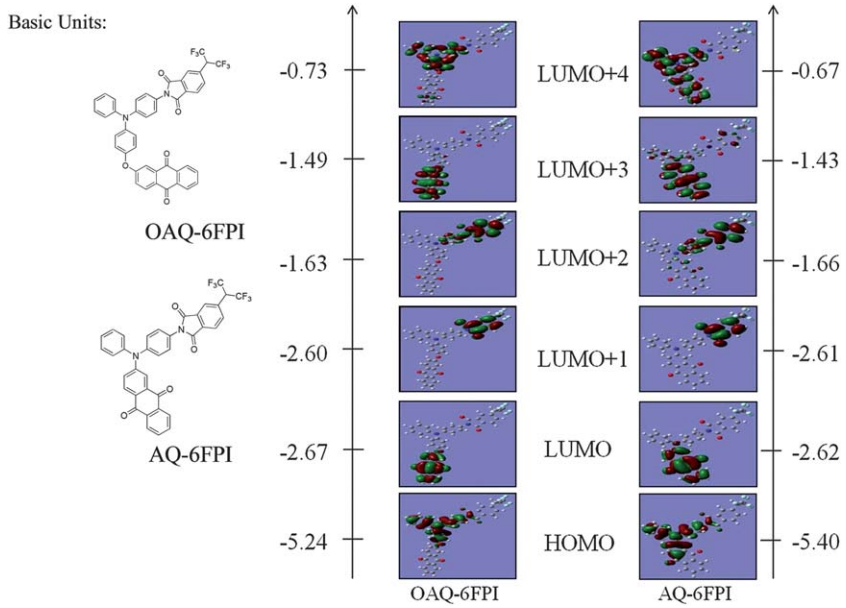

Fig. 5 Calculated molecular orbitals and the corresponding energy levels of the basic units (BU) for **OAQ-6PFI** and **AQ-6FPI**.

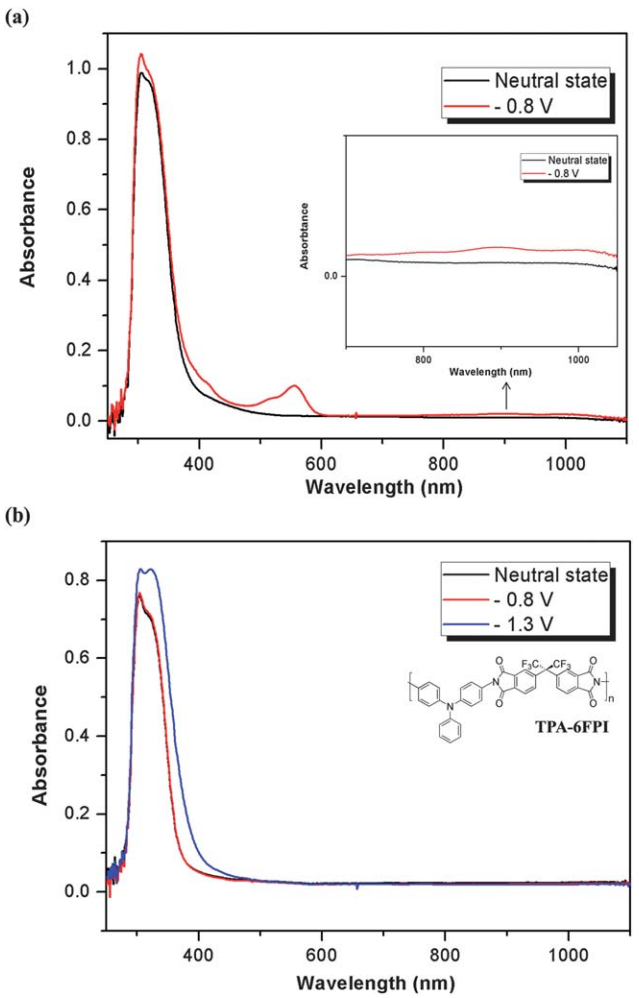

Fig. 6 UV-vis-NIR spectra of polyimide (a) **OAQ-6FPI** (b) **TPA-6FPI** thin film on the ITO-coated glass substrate in 0.1 M TBAP/DMF.

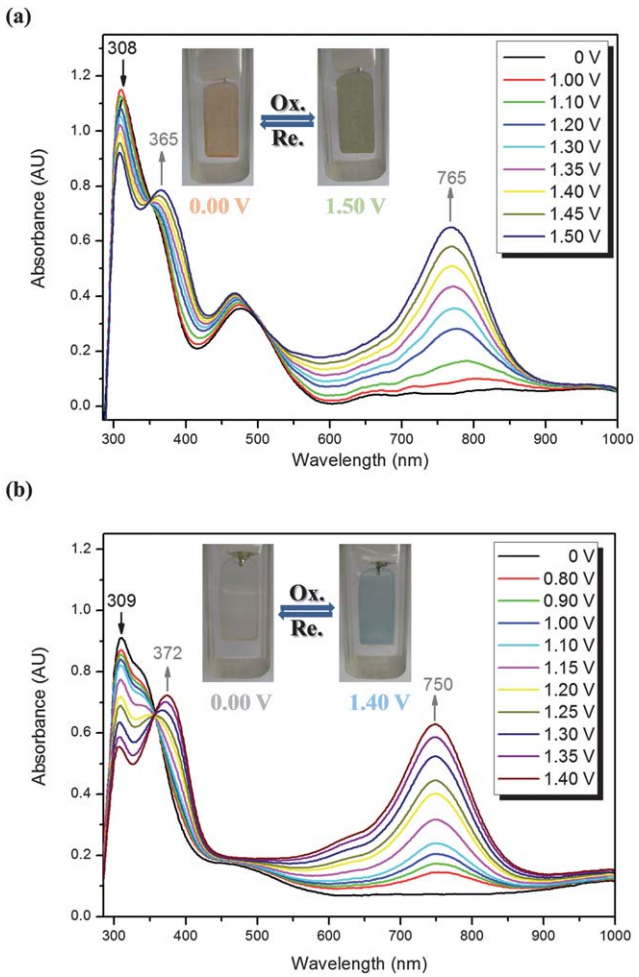

Fig. 7 Electrochromic behavior of polyimide (a) **AQ-DSPI** (b) **OAQ-DSPI** thin film (~65 nm in thickness) on the ITO-coated glass substrate (coated area: 1.6 × 0.6 cm) in 0.1 M TBAP/CH_3CN.

isolated ether linkage switches from almost colorless at the neutral state to blue color during the oxidation scan.

Gas separation

Gas permeability measurements were carried out for polyimide **AQ-6FPI**, **OAQ-6FPI**, and **OAQ-DSPI** membranes prepared by dissolving about 0.8 g of the polyimide sample in 15 mL of DMAc on 12 cm glass Petri dish. The polymer solution was placed at room temperature for 8 h to remove most of the solvent then the semi-dried film was further dried *in vacuo* at 160 °C for 8 h. The thickness of the resulting films was about 50–90 μm, and gas permeability was measured according to the following equation:

$$P = l/(p_1 - p_2) \times \frac{q/t}{A}$$

where P is the gas permeability [cm^3(STP) cm cm^{-2} s^{-1} cmHg], q/t is the volumetric flow rate of the gas permeate [cm^3(STP) s^{-1}], l is the free-standing film thickness (cm), A is the effective free-standing film area (cm^2), and p_1 and p_2 are the pressures (cmHg) on the high-pressure and low-pressure sides of the freestanding film, respectively.

Robeson[14] demonstrated an upper bound in double logarithmic plots of selectivity against permeability for a wide range of polymers. Robeson plots (double logarithmic plots) of selectivity *versus* permeability of the **AQ-** and **OAQ-PIs** for CO_2/CH_4 are depicted in Fig. 8. The gas permeability coefficients and the separation factors (α) based on ratios of pure gas permeability coefficients presented for O_2/N_2 and CO_2/CH_4 pairs of the polymer membranes are summarized in Table 5. Increasing in permeability is generally known to be accompanied by decreasing the permselectivity, which is consistent with the well-known permeability/selectivity trade off rule common in strongly size-sieving polymers. However, the polyimide membranes of the **AQ** and **OAQ PIs** exhibited good permeability as well as high selectivity for CO_2/CH_4 separation owing to the intrinsic noncoplanar TPA segments, contorted $-C(CF_3)_2-$ linkages, and especially arising from the polar carbonyl groups contained in the bulky pendent anthraquinone moieties that

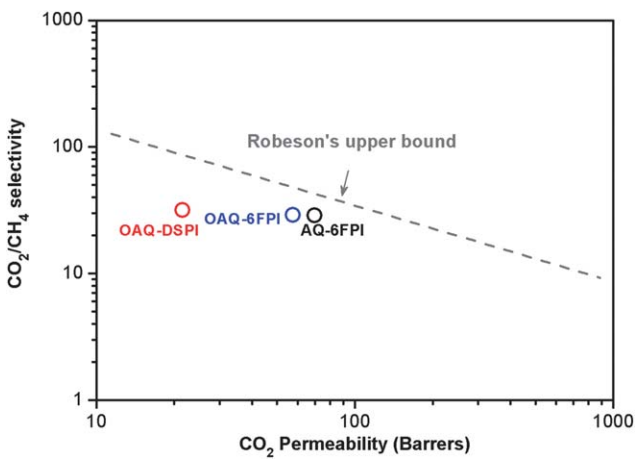

Fig. 8 Double-logarithmic plots of CO_2/CH_4 selectivity *versus* CO_2 permeability for permeable polyimides.

Table 5 Permeability coefficients and ideal separation factors measured at 35 °C and 294 kPa

	Permeation permeabilities (barrier)[a]				Permselectivities ($\alpha_{A/B}$)	
Index	P_{O_2}	P_{N_2}	P_{CO_2}	P_{CH_4}	P_{O_2}/P_{N_2}	P_{CO_2}/P_{CH_4}
AQ-6FPI	2.65	2.36	69.91	2.43	1.12	28.77
OAQ-6FPI	1.56	1.55	57.54	1.98	1.01	29.06
OAQ-DSPI	0.53	0.31	21.56	0.68	1.71	31.71

[a] Permeability values are given in units of barrers, where 1 barrer = $10^{-10}$$cm^3$ (STP) cm/(cm^2 s cmHg), (thickness: 55–90 μm).

hinder intra-segmental mobility, disrupt inter-chain-packing, and increase the interaction capability of CO_2.[15] In addition, it is also revealed that **AQ-6FPI** has higher permeability than **OAQ-6FPI**; this phenomenon could be attributed to the bulky substituent being attached to the backbone directly for **AQ-6FPI** rather than *via* a ether spacer linkage to the main chain for **OAQ-6FPI**, which was also demonstrated in the Si-substituted glassy polymer system in a previous report.[16]

Conclusion

TPA-based aromatic polyimides containing pendent anthraquinone both directly attached to and incorporated *via* ether linkage into backbone as electron acceptor have been successfully synthesized for memory devices, electrochromic and gas separation applications. All polyimides exhibited excellent thermal stability and high glass transition temperature. The memory devices with configuration of ITO/**AQ-6FPI**/Al exhibited distinct volatile memory characteristics of DRAM while the ITO/**OAQ-6FPI**/Al showed volatile SRAM memory property. Thus, the results indicated the isolated D–A system could effectively extend the retention time in the memory device application. The ON/OFF current ratios of these memory devices are up to 10^9. The theoretical analysis results, electrochemical and spectroelectrochemical studies suggest that the CT mechanism could be used to explain the memory characteristics of these polyimides, and the linkage effect between the donor and acceptor was also demonstrated.

These electroactive polyimide films also exhibit interesting ambipolar electrochromic characteristics; **OAQ-DSPI** showed a color change from colorless (neutral from) to blue (oxidized from) with large color contrast, and also exhibited an obvious change in UV-vis absorption during the reduction process for **OAQ-6FPI**, which demonstrated the potential of these D–A containing polyimides for not only memory device application but also electrochromic fabrication. Besides, the permeability of CO_2 and CO_2/CH_4 selectivity of these polyimides could be enhanced more effectively by attaching the bulky and carbonyl-containing anthraquinone group directly to the backbone than is incorporated *via* a spacer. Thus, these novel high performance polyimides could be considered as facile and multi-functional materials.

Acknowledgements

The authors are grateful to the National Science Council of Taiwan for financial support of this work. We gratefully

acknowledge C. W. Lu at the Instrumentation Center of National Taiwan University for CHNS (EA) analysis experiments.

References and notes

1 (*a*) R. H. Friend, R. W. Gymer, A. B. Holmes, J. H. Burroughes, R. N. Marks, C. Taliani, D. D. C. Bradley, D. A. Dos Santos, J. L. Bredas, M. Logdlund and W. R. Salaneck, *Nature*, 1999, **397**, 121; (*b*) Q. Peng, E. T. Kang, K. G. Neoh, D. Xiaob and D. Zou, *J. Mater. Chem.*, 2006, **16**, 376; (*c*) K. Lee, J. Y. Kim, S. H. Park, S. H. Kim, S. Cho and A. J. Heeger, *Adv. Mater.*, 2007, **19**, 2445; (*d*) Y. Shao, G. C. Bazan and A. J. Heeger, *Adv. Mater.*, 2008, **20**, 1191; (*e*) Y. Shao, X. Gong, A. J. Heeger, M. Liu and A. K. Y. Jen, *Adv. Mater.*, 2009, **21**, 1972.

2 (*a*) H. Sirringhaus, N. Tessler and R. H. Friend, *Science*, 1998, **280**, 1741; (*b*) L. L. Chua, J. Zaumseil, J. F. Chang, E. C. W. Ou, P. K. H. Ho, H. Sirringhaus and R. H. Friend, *Nature*, 2005, **434**, 194; (*c*) A. Babel, Y. Zhu, K. F. Cheng, W. C. Chen and S. A. Jenekhe, *Adv. Funct. Mater.*, 2007, **17**, 2542; (*d*) M. Morana, M. Wegscheider, A. Bonanni, N. Kopidakis, S. Shaheen, M. Scharber, Z. Zhu, D. Waller, R. Gaudiana and C. Brabec, *Adv. Funct. Mater.*, 2008, **18**, 1757; (*e*) H. Yan, Z. H. Chen, Y. Zheng, C. Newman, J. R. Quinn, F. Dotz, M. Kastler and A. Facchetti, *Nature*, 2009, **457**, 679-U1; (*f*) J. H. Tsai, W. Y. Lee, W. C. Chen, C. Y. Yu, G. W. Hwang and C. Ting, *Chem. Mater.*, 2010, **22**, 3290; (*g*) C. J. Lin, W. Y. Lee, C. Lu, H. W. Lin and W. C. Chen, *Macromolecules*, 2011, **44**, 9565.

3 (*a*) G. Yu, J. Gao, J. C. Hummelen, F. Wudl and A. J. Heeger, *Science*, 1995, **270**, 1789; (*b*) C. J. Brabec, N. S. Sariciftci and J. C. Hummelen, *Adv. Funct. Mater.*, 2001, **11**, 15; (*c*) M. H. Chen, J. Hou, Z. Hong, G. Yang, S. Sista, L. M. Chen and Y. Yang, *Adv. Mater.*, 2009, **21**, 4238; (*d*) J. H. Hou, T. L. Chen, S. Q. Zhang, L. J. Huo, S. Sista and Y. Yang, *Macromolecules*, 2009, **42**, 9217; (*e*) A. Kumar, H. H. Liao and Y. Yang, *Org. Electron.*, 2009, **10**, 1615; (*f*) S. Sista, Z. R. Hong, M. H. Park, Z. Xu and Y. Yang, *Adv. Mater.*, 2010, **22**, E77.

4 (*a*) Q. D. Ling, F. C. Chang, Y. Song, C. X. Zhu, D. J. Liaw, D. S. H. Chan, E. T. Kang and K. G. Neoh, *J. Am. Chem. Soc.*, 2006, **128**, 8732; (*b*) S. G. Hahm, S. Choi, S. H. Hong, T. J. Lee, S. Park, D. M. Kim, W. S. Kwon, K. Kim, O. Kim and M. Ree, *Adv. Funct. Mater.*, 2008, **18**, 3276; (*c*) S. G. Hahm, S. Choi, S. H. Hong, T. J. Lee, S. Park, D. M. Kim, J. C. Kim, W. Kwon, K. Kim, M. J. Kim, O. Kim and M. Ree, *J. Mater. Chem.*, 2009, **19**, 2207; (*d*) K. Kim, S. Park, S. G. Hahm, T. J. Lee, D. M. Kim, J. C. Kim, W. Kwon, Y. G. Ko and M. Ree, *J. Phys. Chem. B*, 2009, **113**, 9143; (*e*) Y. L. Liu, Q. D. Ling, E. T. Kang, K. G. Neoh, D. J. Liaw, K. L. Wang, W. T. Liou, C. X. Zhu and D. S. H. Chan, *J. Appl. Phys.*, 2009, **105**, 044501; (*f*) Y. L. Liu, K. L. Wang, G. S. Huang, C. X. Zhu, E. S. Tok, K. G. Neoh and E. T. Kang, *Chem. Mater.*, 2009, **21**, 3391; (*g*) Y. Q. Li, R. C. Fang, A. M. Zheng, Y. Y. Chu, X. Tao, H. H. Xu, S. J. Ding and Y. Z. Shen, *J. Mater. Chem.*, 2011, **21**, 15643; (*h*) Y. Q. Li, R. C. Fang, S. J. Ding and Y. Z. Shen, *Macromol. Chem. Phys.*, 2011, **212**, 2360; (*i*) C. L. Liu and W. C. Chen, *Polym. Chem.*, 2011, **2**, 2169; (*j*) C. J. Chen, H. J. Yen, W. C. Chen and G. S. Liou, *J. Polym. Sci., Part A: Polym. Chem.*, 2011, **49**, 3709; (*k*) Y. Q. Li, Y. Y. Chu, R. C. Fang, S. J. Ding, Y. L. Wang, Y. Z. Shen and A. M. Zheng, *Polymer*, 2012, **53**, 229; (*l*) B. L. Hu, F. Zhuge, X. J. Zhu, S. S. Peng, X. X. Chen, L. Pan, Q. Yan and R. W. Li, *J. Mater. Chem.*, 2012, **22**, 520; (*m*) Y. G. Ko, W. Kwon, H. J. Yen, C. W. Chang, D. M. Kim, K. Kim, S. G. Hahm, T. J. Lee, G. S. Liou and M. Ree, *Macromolecules*, 2012, **45**, 3749; (*n*) C. J. Chen, H. J. Yen, W. C. Chen and G. S. Liou, *J. Mater. Chem.*, 2012, **22**, 14085.

5 (*a*) D. W. Mosley, K. Auld, D. Conner, J. Gregory, X. Q. Liu, A. Pedicini, D. Thorsen, M. Wills, G. Khanarian and E. S. Simon, *Proc. SPIE–Int. Soc. Opt. Eng.*, 2008, **6910**, 691017; (*b*) Y. Chen, B. Zhang, G. Liu, X. Zhuang and E. T. Kang, *Chem. Soc. Rev.*, 2012, **41**, 4688.

6 A. D. McNaught and A. Wilkinson, *IUPAC Compendium of Chemical Terminology*, 2nd edn, Blackwell Science, 1997.

7 (*a*) T. J. Lee, C. W. Chang, S. G. Hahm, K. Kim, S. Park, D. M. Kim, J. Kim, W. S. Kwon, G. S. Liou and M. Ree, *Nanotechnology*, 2009, **20**, 135204; (*b*) D. M. Kim, S. Park, T. J. Lee, S. G. Hahm, K. Kim, J. C. Kim, W. Kwon and M. Ree, *Langmuir*, 2009, **25**, 11713.

8 (*a*) Q. D. Ling, D. J. Liaw, E. Y. H. Teo, C. X. Zhu, D. S. H. Chan, E. T. Kang and K. G. Neoh, *Polymer*, 2007, **48**, 5182; (*b*) N. H. You, C. C. Chueh, C. L. Liu, M. Ueda and W. C. Chen, *Macromolecules*, 2009, **42**, 4456; (*c*) T. Kuorosawa, C. C. Chueh, C. L. Liu, T. Higashihara, M. Ueda and W. C. Chen, *Macromolecules*, 2010, **43**, 1236.

9 (*a*) K. L. Wang, Y. L. Liu, J. W. Lee, K. G. Neoh and E. T. Kang, *Macromolecules*, 2010, **43**, 7159; (*b*) K. L. Wang, Y. L. Liu, I. H. Shih, K. G. Neoh and E. T. Kang, *J. Polym. Sci., Part A: Polym. Chem.*, 2010, **48**, 5790; (*c*) G. Liu, B. Zhang, Y. Chen, C. X. Zhu, L. Zeng, D. S. H. Chan, K. G. Neoh, J. Chen and E. T. Kang, *J. Mater. Chem.*, 2011, **21**, 6027; (*d*) B. Zhang, G. Liu, C. Wang, K. G. Neoh, T. Bai and E. T. Kang, *ChemPlusChem*, 2012, **77**, 74.

10 (*a*) S. H. Cheng, S. H. Hsiao, T. H. Su and G. S. Liou, *Macromolecules*, 2005, **38**, 307; (*b*) T. H. Su, S. H. Hsiao and G. S. Liou, *J. Polym. Sci., Part A: Polym. Chem.*, 2005, **43**, 2085; (*c*) C. W. Chang, G. S. Liou and S. H. Hsiao, *J. Mater. Chem.*, 2007, **17**, 1007; (*d*) G. S. Liou and C. W. Chang, *Macromolecules*, 2008, **41**, 1667; (*e*) S. H. Hsiao, G. S. Liou, Y. C. Kung and H. J. Yen, *Macromolecules*, 2008, **41**, 2800; (*f*) C. W. Chang, C. H. Chung and G. S. Liou, *Macromolecules*, 2008, **41**, 8441; (*g*) C. W. Chang and G. S. Liou, *J. Mater. Chem.*, 2008, **18**, 5638; (*h*) C. W. Chang, H. J. Yen, K. Y. Huang, J. M. Yeh and G. S. Liou, *J. Polym. Sci., Part A: Polym. Chem.*, 2008, **46**, 7937; (*i*) H. J. Yen and G. S. Liou, *Chem. Mater.*, 2009, **21**, 4062; (*j*) S. H. Hsiao, G. S. Liou and H. M. Wang, *J. Polym. Sci., Part A: Polym. Chem.*, 2009, **47**, 2330; (*k*) G. S. Liou, H. Y. Lin and H. J. Yen, *J. Mater. Chem.*, 2009, **19**, 7666; (*l*) G. S. Liou and H. Y. Lin, *Macromolecules*, 2009, **42**, 125; (*m*) L. T. Huang, H. J. Yen, C. W. Chang and G. S. Liou, *J. Polym. Sci., Part A: Polym. Chem.*, 2010, **48**, 4747; (*n*) H. J. Yen, S. M. Guo and G. S. Liou, *J. Polym. Sci., Part A: Polym. Chem.*, 2010, **48**, 5271; (*o*) H. J. Yen and G. S. Liou, *J. Mater. Chem.*, 2010, **20**, 9886; (*p*) H. J. Yen, H. Y. Lin and G. S. Liou, *Chem. Mater.*, 2011, **23**, 1874; (*q*) H. J. Yen, S. M. Guo, G. S. Liou, J. C. Chung, Y. C. Liu, Y. F. Lu and Y. Z. Zeng, *J. Polym. Sci., Part A: Polym. Chem.*, 2011, **49**, 3805; (*r*) L. T. Huang, H. J. Yen and G. S. Liou, *Macromolecules*, 2011, **44**, 9595; (*s*) H. J. Yen and G. S. Liou, *Polym. Chem.*, 2012, **3**, 255; (*t*) L. T. Huang, H. J. Yen, J. H. Wu and G. S. Liou, *Org. Electron.*, 2012, **13**, 840.

11 (*a*) H. J. Yen, S. M. Guo, J. M. Yeh and G. S. Liou, *J. Polym. Sci., Part A: Polym. Chem.*, 2011, **49**, 3637; (*b*) T. J. Lee, Y. G. Ko, H. J. Yen, K. Kim, D. M. Kim, W. Kwon, S. G. Hahm, G. S. Liou and M. Ree, *Polym. Chem.*, 2012, **3**, 1276.

12 Y. W. Liu, Y. Zhang, Q. Lan, S. W. Liu, Z. X. Qin, L. G. Chen, C. Y. Zhao, Z. G. Chi, J. R. Xu and J. Economy, *Chem. Mater.*, 2012, **24**, 1212.

13 H. J. Yen, K. Y. Lin and G. S. Liou, *J. Polym. Sci., Part A: Polym. Chem.*, 2012, **50**, 61.

14 (*a*) L. M. Robeson, *J. Membr. Sci.*, 1991, **62**, 165; (*b*) L. M. Robeson, W. F. Borgoyne, M. Langsam, A. C. Savoca and C. F. Tien, *Polymer*, 1994, **35**, 4970; (*c*) L. M. Robeson, *Curr. Opin. Solid State Mater. Sci.*, 1999, **4**, 549; (*d*) L. M. Robeson, *J. Membr. Sci.*, 2008, **320**, 390.

15 (*a*) C. H. Jung and Y. M. Lee, *Macromol. Res.*, 2008, **16**, 555; (*b*) X. Ma, R. Swaidan, Y. Belmabkhout, Y. Zhu, E. Litwiller, M. Jouiad, I. Pinnau and Y. Han, *Macromolecules*, 2012, **45**, 3841.

16 Y. Yampolskii, *Macromolecules*, 2012, **45**, 3298.

